Intermolecular β-sheet formation guides the interaction between ubiquitin-like modifier FAT10 and adapter protein NUB1L

Charlotte Weiss,[1] Nicola Catone,[2] Sarah Overall,[3] Alexander B. Barnes,[3] Annette Aichem,[2] Marcus Groettrup,[4] and Guinevere Mathies[1,*]

[1]Department of Chemistry, University of Konstanz, 78464 Konstanz, Germany

[2]Institute of Cell Biology and Immunology Thurgau, 8280 Kreuzlingen, Switzerland

[3]Department of Chemistry and Applied Biosciences, ETH Zürich, 8093 Zürich, Switzerland

[4]Division of Immunology, Department of Biology, University of Konstanz, 78464 Konstanz, Germany

ABSTRACT

Under inflammatory conditions, the ubiquitin-like modifier FAT10 targets proteins for rapid and irreversible degradation by the 26S proteasome. FAT10 is degraded along with its substrates; in this process, the weak folding of FAT10 and the adapter protein NUB1L are believed to play crucial roles. We report the investigation of the N-domain of FAT10 and its interaction with NUB1L by magic-angle spinning (MAS) nuclear magnetic resonance (NMR) spectroscopy. A stretch of residues that is unobserved when the N-domain of FAT10 is in its ubiquitin-like β-grasp fold, becomes part of an intermolecular β-sheet upon binding to NUB1L. The rest of the N-domain is stabilized in a disordered state, with exception of a series of anchor residues and the N-terminus. MAS NMR is thus able to experimentally capture, at the atomic level, the shapeshifting of FAT10. Binding of the N-terminus likely plays a critical role in the presentation of the unfolded N-domain to the proteasome.

INTRODUCTION

The protein FAT10 (human leukocyte antigen F adjacent transcript 10) consists of two ubiquitin-like (UBL) domains, often referred to as the N- and the C-domain. Its gene was first identified in 1996 by sequencing of the human major histocompatibility complex class I locus,[1] suggesting a role in the immune response. Indeed, FAT10, which is unique to mammals, is mainly present in cells and organs of the immune system.[2–4] In other cell types and tissues, expression of FAT10 is strongly upregulated by the proinflammatory cytokines tumor necrosis factor-α and interferon-γ.[5,6] FAT10 plays a role in adaptive as well as innate immune responses, affecting, for example, peptide presentation[7] and autophagy[8] — the list of confirmed covalent and non-covalent binding partners continues to grow.[9] FAT10 has been shown to be upregulated in at least a dozen types of cancer and appears to have a positive impact on metastasis.[3,10] Conversely, disruption of the interaction of FAT10 with MAD2 (mitotic arrest deficient 2) has been shown to inhibit tumor progression.[11]

While many of the functions of FAT10 have been investigated only superficially, it is well established that FAT10 targets proteins for degradation by the 26S proteasome.[12] Just like ubiquitylation, FAT10ylation requires a conjugation cascade involving three enzyme types: E1 activating enzyme UBA6[13,14], E2 conjugating enzyme USE1[15] (and several others)[16], and E3 ligase Parkin[17]. FAT10 is capable of activating all proteolytic activities of the proteasome, but only together with its binding partner NUB1L, the long isoform of NEDD8-ultimate buster 1.[18,19] Recently, it was found that interaction with the N-domain of FAT10 increases the affinity of NUB1L for the RPN1 subunit of the 19S regulatory particle of the proteasome.[20]

Unlike ubiquitin, FAT10 is degraded along with its substrates and, with a half-life in cells of 1 h, it is extremely short-lived.[12] In combination with fast upregulation, this makes FAT10 a tool for prompt but time-limited responses to harmful factors during inflammatory processes.[9] The weak folding of FAT10 has long been suspected to be critical for its biological function. The segregase VCP (valosin containing protein, also known as p97) is required for proteasomal degradation of ubiquitylated proteins that lack a disordered initiation region, but degradation of FAT10 or FAT10ylated proteins is VCP independent.[21] FAT10 melts at a temperature of 41 °C (compared to 83 °C for ubiquitin)[21] and shows poor solubility[22,23]. The latter property has interfered with structural investigations over the years. Theng *et al.* eventually determined, by liquid-state NMR, a structure of the N-domain after deletion of seven N-terminal residues.[11] Later, Aichem *et al.* succeeded in determining the structure of a stabilized, Cys-free mutant of FAT10 by X-ray crystallography (for the N-domain) and liquid-state NMR (for the C-domain).[21] Both domains show the β-grasp fold of ubiquitin[24], but their surfaces differ from ubiquitin and each other. The Cys-free mutant was found to be well conjugated, but, confirming suspicions, was degraded at a much slower pace. This raises the question of how the weak folding of FAT10 enables fast degradation and why interaction with NUB1L is essential.

We report here the investigation of the N-domain of FAT10 and its interaction with NUB1L by magic-angle spinning (MAS) NMR spectroscopy. MAS NMR is not restricted by molecular size, solubility or a disorderly arrangement of structural units and can, in addition to inter-atomic distances, probe local chemical environments and motion. This makes MAS NMR well-suited for the atomic-level exploration of interactions between biomolecules, even if one or more binding partners are weakly folded. Recent examples include structural characterization of branching stimulant

TPX2 (targeting protein for Xklp2), which forms condensates upon binding to microtubules, but is disordered in solution[25] and the observation of a paired helical filament fold of the intrinsically disordered tau protein bound to lipid membranes[26]. Co-sedimentation by ultracentrifugation is often a good strategy to form biomolecular complexes in the MAS rotor.[27,28]

We start by examining the isolated N-domain of Cys-free FAT10 (N-FAT10-C0) in microcrystalline form. Sequential assignment of resonances is possible for 69 out of 83 residues; not observed are the flexible start and end tails and residues I68-I74. Torsion angles and secondary structure predictions based on chemical shifts are in agreement with the crystal structure[21]. Next, we examine, as a physiologically relevant reference sample, isolated lyophilized and rehydrated N-FAT10-C0. Backbone connectivity is reduced, but with help from the chemical shifts of the microcrystalline sample, sequential assignment remains possible. Predicted torsion angles are similar to the microcrystalline form, but the stretch of unobserved residues is lengthened to I68-L76. Finally, we turn to N-FAT10-C0 co-sedimented with NUB1L. The spectra show a drastically reduced number of resonances, which are confidently assigned to residues I68-V81 and the N-terminus of N-FAT10-C0. We attribute the disappearance of the other residues to disorder. Analysis of chemical shifts indicates that residues T73-V81 of N-FAT10-C0 constitute a β-strand, which provides experimental evidence for AlphaFold-Multimer[29] predictions that suggest the formation of an intermolecular, anti-parallel β-sheet consisting of residues L76-V81 of FAT10 and Y212-N217 of NUB1L. Alphafold-Multimer, however, does not predict the binding of the N-terminus.

MATERIALS and METHODS

Below we give short accounts of all procedures. Further specifics can be found in the Supporting Information.

Expression and Purification of U-^{13}C,^{15}N-N-FAT10-C0. Cys-free N-domain of human FAT10 (amino acids 5-86; C7T, C9T) was expressed as a His_6-GST-fusion protein in *E. coli* BL21-CodonPlus(DE3)-RIPL competent cells (Agilent Technologies). An additional glycine residue at the N-terminus remains from the TEV protease cleavage site. For uniform ^{13}C and ^{15}N labelling, cells were grown in M9 minimal medium supplemented with U-$^{13}C_6$-D-glucose and ^{15}N-ammonium chloride. The purification was adapted from a previously published protocol.[21] Briefly, bacterial cells were lysed and the supernatant was applied to nickel affinity chromatography. After buffer exchange and cleavage of the purification tag, His-tagged TEV protease and byproducts were separated by a second nickel affinity chromatography. Final purification by size-exclusion chromatography yielded up to 7 mg per liter of M9 medium.

Expression and Purification of NUB1L. Human NUB1L (amino acids 2-615) was expressed as a His_6-SUMO-fusion protein, also in *E. coli* BL21-CodonPlus(DE3)-RIPL competent cells. To produce natural abundance NUB1L, cells were grown in LB medium. Purification requires the same steps as for U-^{13}C,^{15}N-N-FAT10-C0. Yield was up to 15 mg per liter of LB medium.

Microcrystalline N-FAT10-C0. The crystallization protocol of Aichem *et al.*[21] was taken as a starting point to obtain microcrystals of U-^{13}C,^{15}N-N-FAT10-C0. The sitting drop vapor diffusion method was used, with a crystallization solution of ammonium sulfate at pH 2.5. Microcrystals were packed into the MAS rotor by ultracentrifugation with a

tool manufactured at the workshop of the University of Konstanz following Mandal *et al*.[30] The rotor finally contained an estimated 13.5 mg of protein.

Lyophilized/rehydrated N-FAT10-C0. With its molecular weight of less than 10 kDa, the N-domain of FAT10 is too small to be sedimented into a MAS rotor by ultracentrifugation.[31] To nevertheless obtain a reference sample at physiological pH, U-^{13}C,^{15}N-N-FAT10-C0 was lyophilized from buffer solution (pH 7.5), ground, and manually packed into a rotor, to a total estimated amount of 14.5 mg. To rehydrate, MilliQ water was added in steps of 1 μL until spectral resolution no longer improved.

Complex of N-FAT10-C0 and NUB1L. Binding to NUB1L was previously demonstrated for the wild-type N-domain of FAT10[32], but not for the stabilized, Cys-free version. We therefore verified complex formation of N-FAT10-C0 and NUB1L by size exclusion chromatography (Figure S1). Co-sedimentation by ultracentrifugation, in a molar ratio of 1:1, was used to form the complex of natural abundance NUB1L and U-^{13}C,^{15}N-N-FAT10-C0 in the MAS rotor.

MAS NMR Spectroscopy. Experiments were performed at 18.8 and 20.0 T (^{1}H Larmor frequencies of 800 and 850 MHz) on Bruker Avance NEO/III spectrometers, each equipped with a 3.2 mm E-free HCN Bruker MAS probe. The spinning frequency was 14.5 or 19.0 kHz. The sample temperature was 4 °C, unless noted otherwise. Chemical shifts of ^{13}C are referenced to DSS in D_2O (0.5% by weight), chemical shifts of ^{15}N are referenced to liquid ammonia at 25 °C.

Sample integrity was verified by ^{1}H-^{13}C and ^{1}H-^{15}N cross polarization experiments as well as ^{13}C-^{13}C correlation spectra recorded with the dipolar assisted rotational resonance (DARR) pulse sequence.[33] The mixing time was set to 10.0 ms to observe primarily one- and two-bond correlations. From ^{13}C-^{13}C correlation patterns, amino acid residue types can be identified, but sequential assignment is not possible. For this purpose, ^{15}N-^{13}C and ^{15}N-^{13}C-^{13}C spectra were recorded with the *z*-filtered transferred echo double-resonance (ZF TEDOR)[34] and the ZF TEDOR DARR[35] pulse sequences, respectively. The TEDOR mixing time was set to ~1 ms to emphasize N-C_α and N-C' magnetization transfers along the protein backbone and, in the sidechains, to carbon nuclei directly bonded to nitrogen nuclei. The DARR mixing time in these experiments was set to 40-50 ms to enable transfer from the C_α and C' nuclei to other carbon nuclei within a residue.

The ZF TEDOR DARR sequence provides NCACX and NCOCX connectivities within one 3-dimensional spectrum, but at the cost of large spectral widths. To keep the number of increments in the indirect dimensions under control, it sufficed for microcrystalline N-FAT10-C0 to truncate the free induction decay along the indirect ^{13}C dimension and pad it using linear forward prediction. For lyophilized/rehydrated N-FAT10-C0 and the N-FAT10-C0/NUB1L complex, we used aliasing. At a spinning frequency of 19 kHz, a convenient strategy is to set the dwell time of the indirect ^{13}C dimension equal to one rotor period and the carrier frequency to approximately 50 ppm.[36] The carbonyl resonances are now observed at the positions of their spinning sidebands just above the aliphatic region. A supplementary NCOCX measurement with SPECIFIC-CP[37] and combined $R2_n^\nu$-driven (CORD)[38] ^{13}C-^{13}C mixing provided additional connections for lyophilized/rehydrated N-FAT10-C0.

An overview of all MAS NMR experiments and acquisition parameters is given in Tables S1 and S2. Spectra were processed in TopSpin or NMRPipe[39]. CcpNmr Analysis was used for the resonance assignments.[40,41]

Torsion Angle and Secondary Structure prediction. Backbone torsion angles Φ and Ψ and secondary structure were predicted empirically based on chemical shifts of assigned N, C', C_α, and C_β nuclei.[42,43] For this purpose, we used TALOS-N,[44] which combines a set of trained neural networks with efficient mining of a database of proteins of which both the X-ray structure and the chemical shifts are known.

AlphaFold Modelling. The structure of isolated N-FAT10-C0 (amino acids 5-86 with C7T and C9T and the additional glycine at the N-terminus) was predicted with AlphaFold[45] v2.3.2 (reduced database). The maximum template release date was 2014-08-26. Five predictions were obtained, from one seed per model, and ranked according to the predicted local distance difference test (pLDDT) confidence score; only the best prediction was relaxed.

The structure of the complex of N-FAT10-C0 and NUB1L (amino acids 1-615) was predicted with AlphaFold-Multimer (reduced database).[29] The maximum template release date was 2004-11-28. Twenty-five predictions were obtained, from five seeds per model, and ranked according to a weighted combination of the predicted template modelling (pTM) and interface pTM scores (model confidence = 0.8·ipTM + 0.2·pTM). Only the best prediction was relaxed.

All AlphaFold modelling was performed on the Scientific Compute Cluster of the University of Konstanz (SCCKN). UCSF ChimeraX[46] was used for structure visualization. Torsion angles were extracted from the AlphaFold structures using VADAR.[47]

RESULTS

Valuation of Samples. Figures 1 and S2 show the ^{1}H-^{13}C and ^{1}H-^{15}N cross-polarization spectra of the three samples of N-FAT10-C0. Conformational homogeneity of N-FAT10-C0 in the microcrystals[48,49] leads to well-resolved spectra (bright green); ^{13}C linewidths are 1 ppm or less. Some resonances are skewed, for example, of $^{13}C_{\delta 1}$ of Ile at 9 ppm. This likely reflects distinct conformations of multiple molecules in the unit cell. In the sample of lyophilized/rehydrated N-FAT10-C0 (turquoise spectra), the conformations of the protein are not restricted by crystal packing and resonances have broadened; this is particularly noticeable for the backbone nitrogen atoms. Deprotonation of Asp and Glu has shifted the $^{13}C_\gamma$ and $^{13}C_\delta$ resonances downfield[50,51], changing the appearance of the carbonyl region; for the same reason, the resonance of $^{15}N_{\delta 1}$ of His has shifted downfield, out of the spectral range. Although there are further small changes, the ^{1}H-^{13}C cross-polarization spectra of lyophilized/rehydrated N-FAT10-C0 and of microcrystalline N-FAT10-C0 look very similar. To prepare the third sample, N-FAT10-C0 was co-sedimented with NUB1L. Resolution of the spectra (orange) is good, with ^{13}C linewidths again $\leq$ 1 ppm. Spectral features differ drastically from isolated N-FAT10-C0.

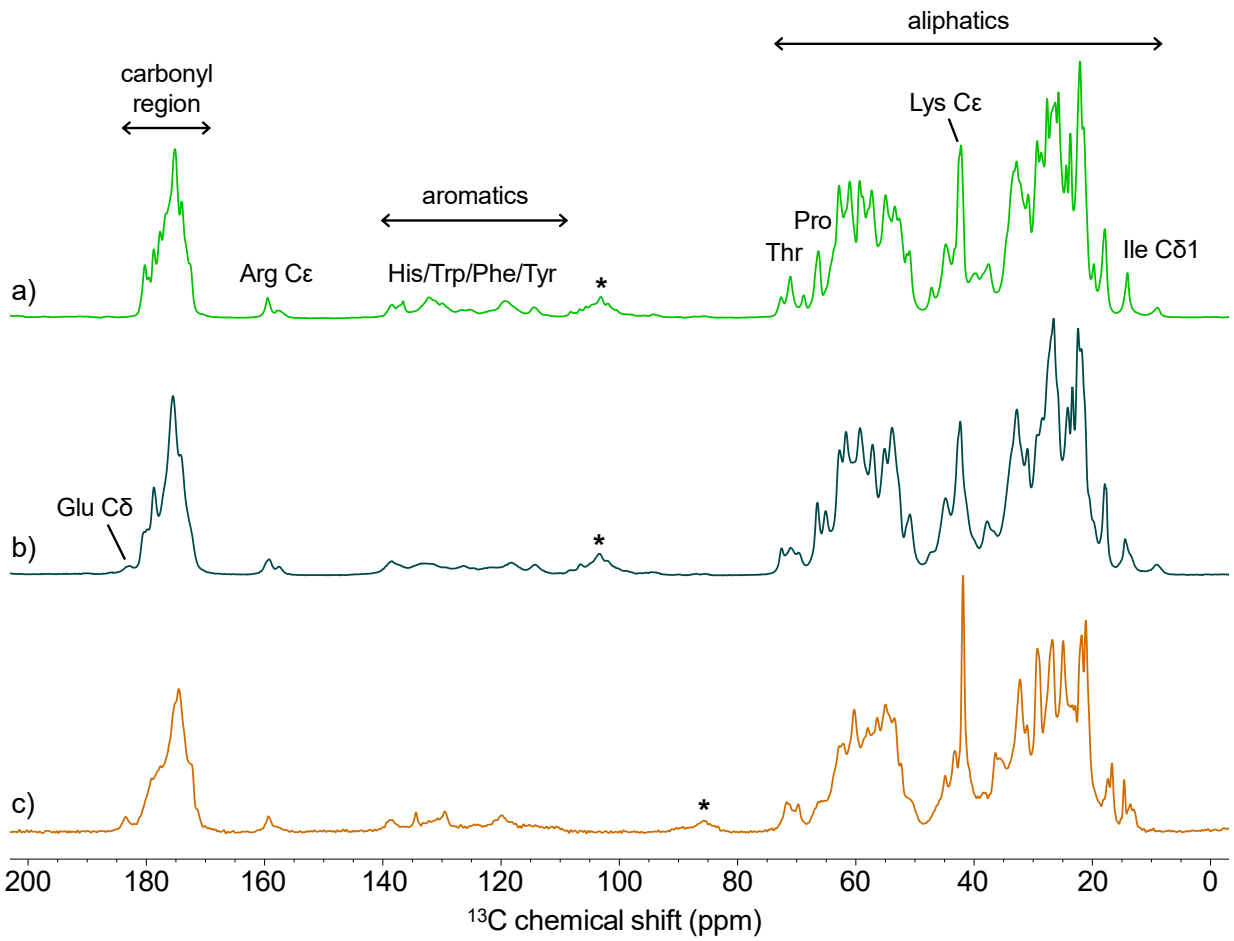

Figure 1. *^{1}H-^{13}C cross-polarization spectra of (a) microcrystalline N-FAT10-C0, (b) lyophilized/rehydrated N-FAT10-C0, and (c) N-FAT10-C0 in complex with NUB1L. Spectra were recorded at 18.8 T with a spinning frequency of 14.5 kHz (a,b) and at 20.0 T with a spinning frequency of 19.0 kHz (c). The sample temperature was 4 °C. The stars indicate spinning sidebands.*

Resonance Assignments and Secondary Structure of Microcrystalline N-FAT10-C0. ^{13}C-^{13}C and ^{15}N-^{13}C correlation spectra of microcrystalline N-FAT10-C0 are shown, along with resonance assignments, in Figures S3a and b. Figure S4 shows a representative strip plot of the ^{15}N-^{13}C-^{13}C spectrum. Connectivity along the backbone is excellent: following the NCA/NCO transfer, side chains are visible up to the ^{13}C$_{\delta}$. In tightly packed regions, magnetization also transfers to ^{13}C nuclei of neighbouring residues, which was helpful to verify sequential assignments. The ^{13}C-^{13}C correlation spectrum is dominated by one- and two-bond transfers, but cross peaks from three-bond transfers are also discernible from the noise. This made for convenient pattern recognition and assisted in the assignment of residues with aromatic carbons or long aliphatic side chains. Some inter-residue contacts, e.g. T9-V10 and G53-S54, are visible. The ^{15}N-^{13}C correlation spectrum served to verify connectivities observed in the three-dimensional spectrum and was helpful for the assignment of residues with a ^{15}N nucleus in the sidechain.

In total, we were able to sequentially assign 69 of the 83 residues of N-FAT10-C0, see Figure 2. For five of these residues, some uncertainty remains (highlighted yellow in Figure 2). The backbone ^{15}N chemical shifts of K32 and K34

and their succeeding residues are nearly identical, making it difficult to tell them apart. The signals from L8, D69, and T73 are very weak. For eight residues, we observed up to three conformations (blue). All unobserved residues (grey) are located in the flexible tails (G4-T7 and K82-E86) and in the stretch I68-I74.

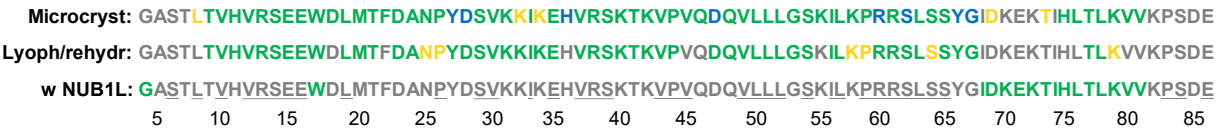

Figure 2. *Overview of sequential assignments of microcrystalline N-FAT10-C0, lyophilized/rehydrated N-FAT10-C0, and N-FAT10-C0 in complex with NUB1L. Green = unambiguous, yellow = ambiguous, blue = multiple conformations, grey = unobserved. Of the grey, underlined residues of N-FAT10-C0 in complex with NUB1L, we observe 1×E, 1×I, 1×L, 1×P, 1×R, 2×S, and 3×V, but sequential assignment was not possible.*

Figure 3 shows the predicted backbone torsion angles Φ and Ψ based on the resonance assignments, together with the torsion angles of the X-ray structure of N-FAT10-C0[21]. Agreement is very good; the root of the mean square deviation is 14° for Φ and 12° for Ψ. Predicted secondary structure elements also match the X-ray structure (Figure S3c).

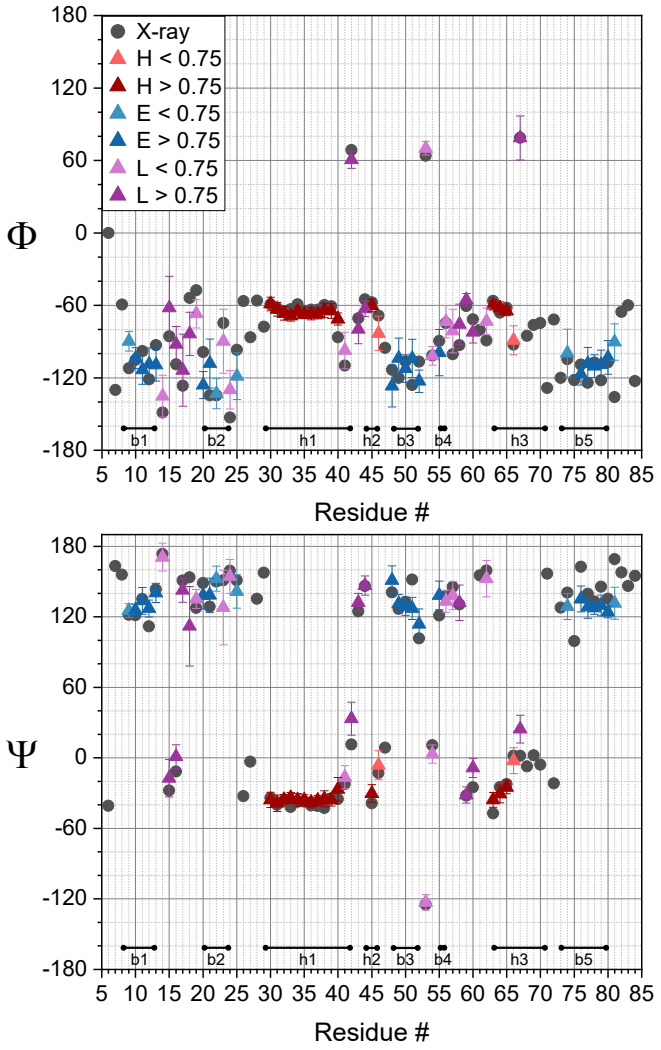

Figure 3. *Backbone torsion angle and secondary structure predictions based on MAS NMR of microcrystalline N-FAT10-C0. Error bars correspond to the standard deviation of the Φ and Ψ angles of the best matches in the TALOS-N database. For residues P26-S29, D47, R61, and H75, there is no consensus among the database matches and, hence, no torsion angles are shown. No predictions are made for L8, I68-T73, and K82. Secondary structure predictions are based on observed chemical shifts except for G67, for which the prediction is based on sequence information, and classified as helix (H), strand (E), or loop (L). Predictions with a confidence > 0.75 are highly reliable. Torsion angles (black dots) and secondary structure elements (b stands for strand and h for helix) of the X-ray structure of N-FAT10-C0 (PDB-ID 6GF1, chain B) are also plotted for comparison.*

Resonance Assignments and Secondary Structure of Lyophilized/Rehydrated N-FAT10-C0. ^{13}C-^{13}C and ^{15}N-^{13}C correlation spectra of lyophilized/rehydrated N-FAT10-C0 are shown, along with resonance assignments, in Figures 4a and b. As expected from the one-dimensional spectra, cross peaks have broadened, but, in the ^{13}C-^{13}C spectrum, sidechain patterns are still readily recognized. Figure S5 shows a representative strip plot of the ^{15}N-^{13}C-^{13}C spectrum. Backbone connectivity is not as good as for the microcrystalline sample. This problem was mitigated by recording an additional NCOCX correlation spectrum (Figure S6), with a narrow spectral width and an increased number of scans.

In total, we sequentially assigned 56 of the 83 residues of N-FAT10-C0 (Figure 2). The assignment was performed *de novo*, but the known chemical shifts of microcrystalline N-FAT10-C0 provided essential guidance. For example, the sidechain patterns of I33 and I56 are very similar in both samples. For residues T21, P26, Y27, L51, L63, and L78, the connectivities were only observed in the additional NCOCX spectrum. Signals from P26 and P56 partially overlap and signals from their preceding residues (N25 and K58) are weak. Hence, these assignments are ambiguous (yellow). The same applies for S64, which overlaps with other serines; the signals from K79 are weak. Residues in the elongated, flexible tails G4-L8 and V80-E86 are not observed, nor is the full stretch I68-L76 (grey), resembling microcrystalline N-FAT10-C0. In addition, residues D18, F22, H36, V45, Q46, and K55 are not observed; possibly multiple conformations of (neighboring) bulky sidechains create local disorder in the backbone.

Comparison of the chemical shifts of the microcrystalline and lyophilized/rehydrated samples of N-FAT10-C0 shows small changes (1-2 ppm) for most nuclei, which tend to be larger, up to 5 ppm, if a neighboring residue is not observed in the lyophilized/rehydrated sample. Vice versa, N-C_α connectivities of W17 and G67 were not observed for the microcrystalline sample, but are visible in the ^{15}N-^{13}C spectrum of the lyophilized/rehydrated sample (Figure 4b) at 59.1,118.8 ppm and 45.9,107.5 ppm, also suggesting that local changes in structure have occurred. Predicted torsion angles and secondary structure (Figure S7) are, however, similar for both samples of isolated N-FAT10-C0, indicating that the overall fold is unchanged. This result is visualized in Figure 4c, where the predicted secondary structure is projected on the AlphaFold structure of N-FAT10-C0.

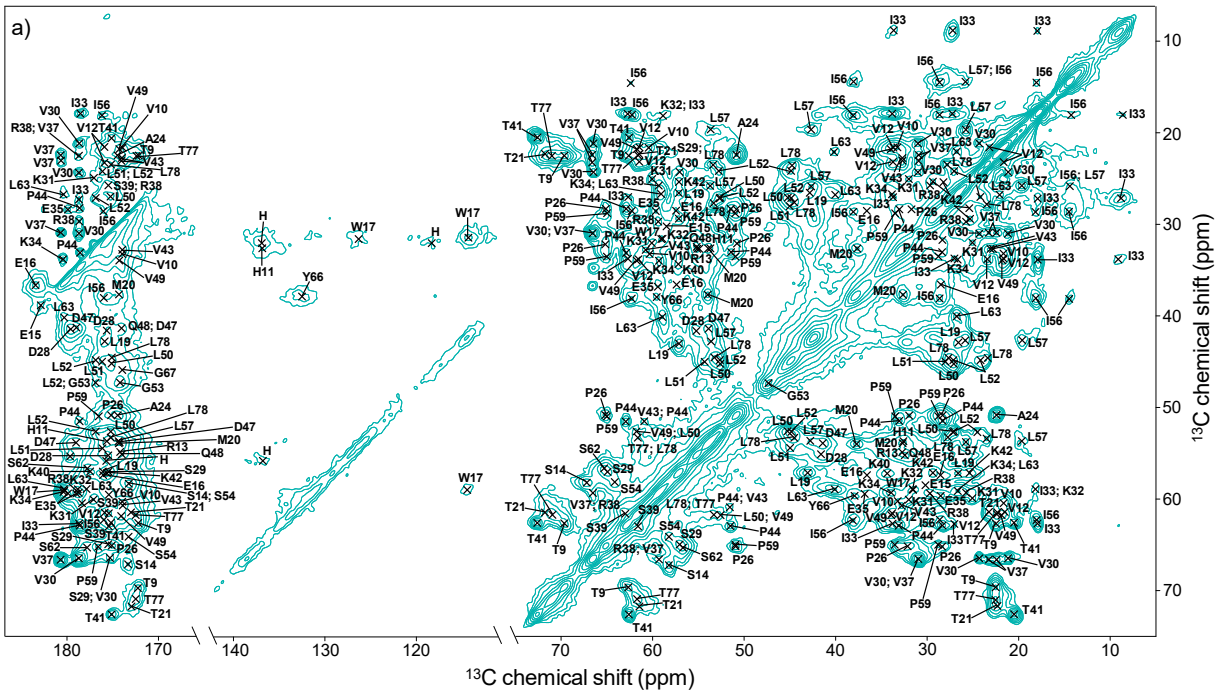
a)
^{13}C chemical shift (ppm)
^{13}C chemical shift (ppm)

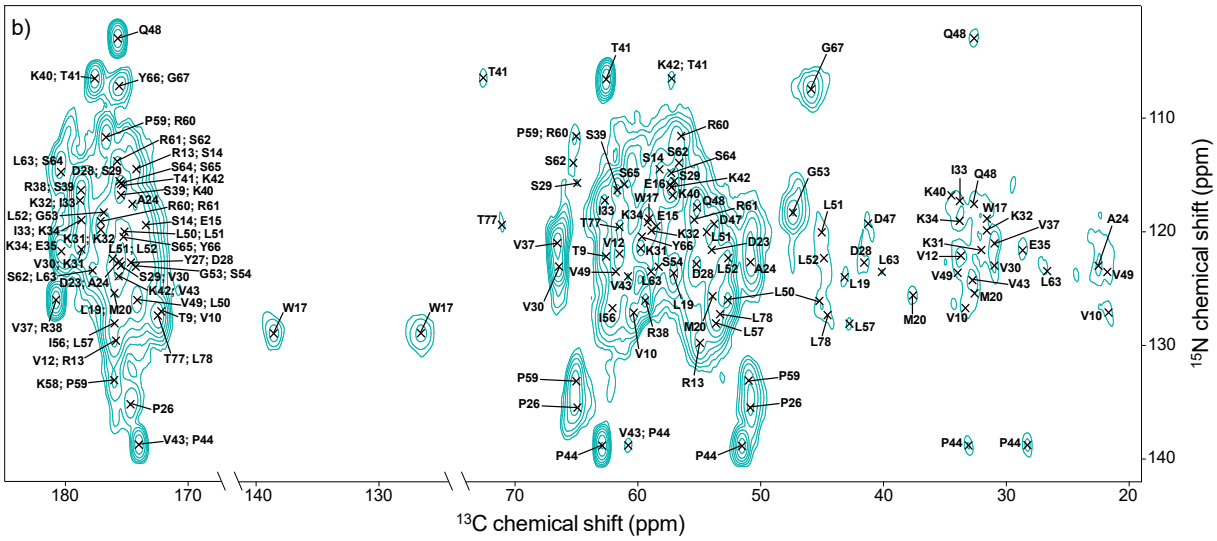
b)
^{13}C chemical shift (ppm)
^{15}N chemical shift (ppm)

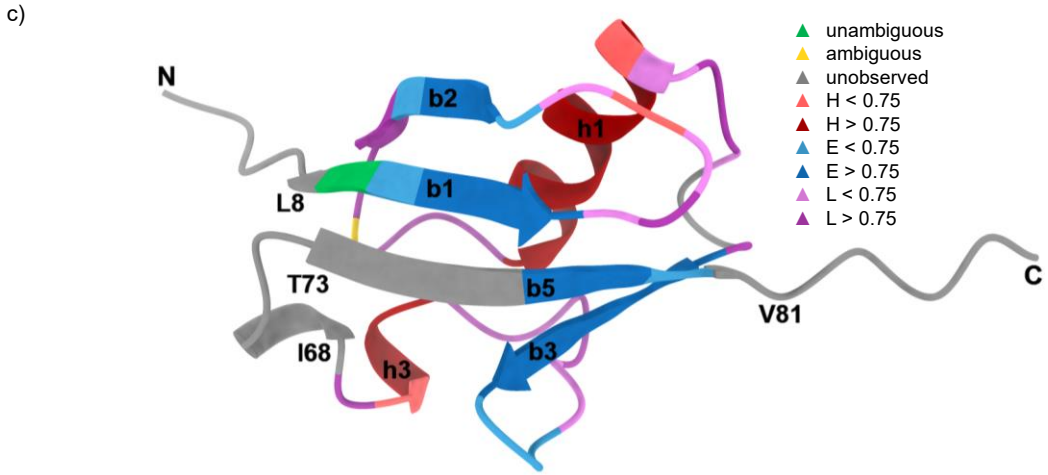
c)
N
C
L8
T73
I68
V81
b1
b2
b3
b5
h1
h3
unambiguous
ambiguous
unobserved
H < 0.75
H > 0.75
E < 0.75
E > 0.75
L < 0.75
L > 0.75

Figure 4. *(a) ^{13}C-^{13}C DARR spectrum and (b) ^{15}N-^{13}C ZF TEDOR spectrum of lyophilized/rehydrated N-FAT10-C0. Sequentially assigned cross peaks are marked and labelled in both spectra. As a result of the relatively long mixing time and the large number of scans for the given amount of protein, two- and three-bond NC_β/NC_γ correlations are visible in the ^{15}N-^{13}C correlation spectrum. Cross peaks from sidechains of His (^{15}N chemical shift 166 ppm), Arg (^{15}N chemical shift 67-90 ppm), and Lys (^{15}N chemical shift 35 ppm) are also observed, but not plotted here. (c) Projection of TALOS-N secondary structure predictions per residue on the AlphaFold structure of N-FAT10-C0. H stands for helix, E for strand, and L for loop. D18, F22, H36 and K55 are unassigned, but secondary structure is predicted from the chemical shifts of neighboring residues. For residues N25, K58, P59, S61 and K79, the assignments are ambiguous, but since the secondary structure is predicted from chemical shifts, they are color coded accordingly. See Figure S7 for plots of the backbone torsion angles and further specifics.*

Interaction of N-FAT10-C0 and NUB1L. Figures 5a and b show the ^{13}C-^{13}C and ^{15}N-^{13}C correlation spectra of N-FAT10-C0 co-sedimented with NUB1L. Compared to the spectra of isolated N-FAT10-C0 (Figures S3a,b and 4a,b), the number of cross peaks is much reduced. In the aforementioned MAS NMR pulse sequences, magnetization transfer relies on dipolar couplings, which can be averaged out by molecular motion. To explore if this is happening here, we measured ^{1}H-^{13}C cross-polarization spectra at reduced temperatures of −2, and −10°C (Figure S8). These spectra, however, show no new signals, only a slight decrease in resolution. We also obtained a ^{13}C spectrum with the liquid-state NMR sequence INEPT (insensitive nuclei enhanced by polarization transfer)[52], which requires J-coupling for magnetization transfer and motion on pico- to nanosecond time scales. Weak signals from mobile parts of sidechains become visible only after a lot of averaging. We surmise that disorder (which may still be dynamic, see the Discussion) renders a large number of amino acid residues indetectable. For the cross peaks that are visible, resolution is good, as is the connectivity; a representative strip plot of the ^{15}N-^{13}C-^{13}C spectrum is shown in Figure S9.

Confident sequential assignment is possible for residues I68-V81 (Figure 2). Intriguingly, the Gly residue at the N-terminus (G4) is visible at 43.8, 26.8 ppm in the ^{15}N-^{13}C spectrum (Figure 5b). Sidechain patterns are evident for eleven residues (1×E, 1×I, 1×L, 1×P, 1×R, 2×S, 3×V, 1×W), but their backbone connectivities could not be observed. Torsion angle and secondary structure predictions based on the chemical shifts of the assigned residues are plotted in Figure S10. Residues D69-E71 form a loop, while residues T73-V81 form a β-strand.

To further explore the interaction between N-FAT10-C0 and NUB1L, we used structure prediction by AlphaFold-Multimer. The best-ranked structure is shown in Figure 5c (confidence scores are provided in Figure S11). N-FAT10-C0 is in an open, partially unfolded state and NUB1L is wrapped around an intermolecular, anti-parallel β-sheet that consists of residues L76-V81 of N-FAT10-C0 and Y212-N217 of NUB1L.

The AlphaFold-Multimer prediction suggests a plausible interpretation of the MAS NMR experimental data. In preparation of rapid degradation by the proteasome, interaction with NUB1L stabilizes N-FAT10-C0 in an unfolded, mostly disordered state. Only the residues visible in the spectra retain a regular structure; those that were sequentially assigned are highlighted in orange in Figure 5c. The inset in Figure 5c shows the TALOS-N secondary structure predictions projected on the AlphaFold-Multimer structure. MAS NMR thus confirms the formation of the intermolecular β-sheet and suggests that it is, in reality, three residues longer (on the side of N-FAT10-C0, residues T73-V81 participate as opposed to L76-V81). The residues of N-FAT10-C0 preceding the β-strand form a loop until

I68. In addition, eleven residues scattered along the N-FAT10-C0 chain plus the Gly N-terminus show conformational homogeneity. We suspect that these residues form anchor points where N-FAT10-C0 interacts non-covalently with NUB1L. Of these, the N-terminus is of particular importance because it is the first residue of the unfolded FAT10 chain to enter the proteasome[12,21,53].

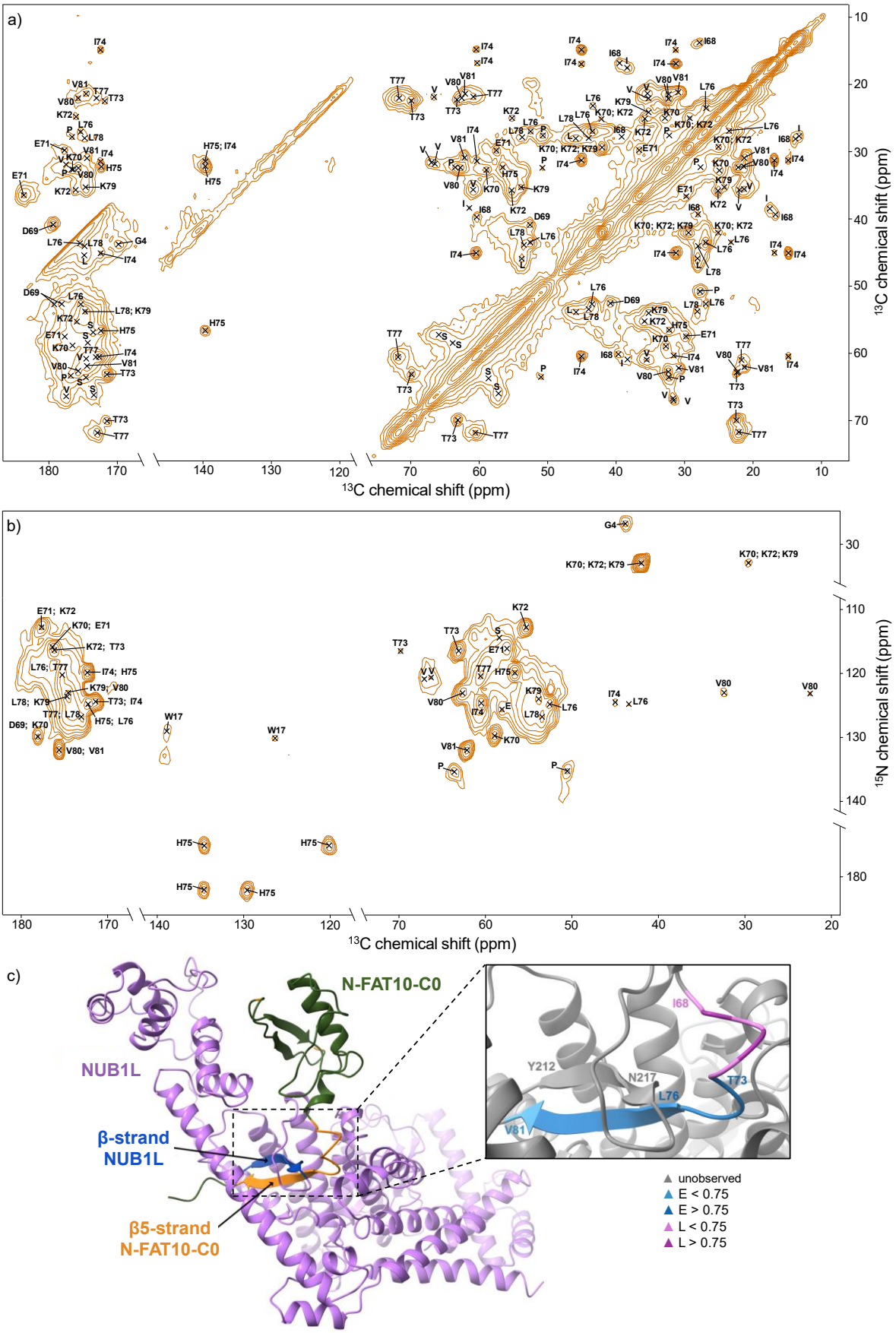
a)
^{13}C chemical shift (ppm)
^{13}C chemical shift (ppm)
b)
^{15}N chemical shift (ppm)
^{13}C chemical shift (ppm)
c)
N-FAT10-C0
NUB1L
β-strand
NUB1L
β5-strand
N-FAT10-C0
I68
Y212
N217
L76
T73
V81
unobserved
E < 0.75
E > 0.75
L < 0.75
L > 0.75

Figure 5. *(a) ^{13}C-^{13}C DARR spectrum and (b) ^{15}N-^{13}C ZF TEDOR spectrum of N-FAT10-C0 co-sedimented with NUB1L. Assigned cross peaks are marked and labelled in both spectra. Cross peaks from sidechains of Arg (^{15}N chemical shift 67-90 ppm) are also observed but not plotted here. (c) AlphaFold-Multimer prediction for the interaction of N-FAT10-C0 and NUB1L. The residues of N-FAT10-C0 that are observed by MAS NMR are highlighted in orange. The inset shows the secondary structure predictions for residues I68-V81 projected on the AlphaFold-Multimer structure (E stands for strand and L for loop). See Figure S10 for the backbone torsion angles and further specifics.*

DISCUSSION

The E1 enzyme UBA6 is unusual in the sense that it not only activates FAT10, but also ubiquitin.[13,14] Co-crystallization of UBA6 with Cys-free FAT10 has revealed that the binding of the C-domain of FAT10 is analogous to the binding of ubiquitin to the, ubiquitin-only, E1 enzyme UBA1.[54] The N-domain of FAT10 interacts with the three-helix bundle of UBA6, with the β-grasp fold intact. The conjugation cascade thus requires FAT10 in properly folded form. The interaction of N-FAT10 with UBA6 bears similarity with the interaction of another ubiquitin-like modifier NEDD8 (neural precursor cell-expressed developmentally down-regulated protein 8) with NUB1L: both interactions require a UBA domain, are polar, and rely on N51 of NEDD8 or the analogous residue K58 in N-FAT10. With this information in mind, we naively expected N-FAT10-C0 to remain folded upon binding to NUB1L. To assess the feasibility of a MAS NMR study, we first prepared a microcrystalline sample of isolated N-FAT10-C0. Next, aiming to gain insight into the binding mode and interface via chemical shift perturbations, we prepared a lyophilized/rehydrated reference sample of N-FAT10-C0 at physiological pH. Sequential assignment of N-FAT10-C0 co-sedimented with NUB1L, however, constituted a plot twist and poignantly showed the shapeshifting of the N-domain of FAT10. This experience illustrates the strength of MAS NMR spectroscopy – the unfolding of N-FAT10-C0 makes co-crystallization with NUB1L unlikely to be successful. In contrast, co-sedimentation in the MAS rotor favors the formation of complexes because complexed molecules are extracted from the bulk solution first.[31]

Earlier this year Arkinson *et al.* reported the investigation of the conformation and solvent accessibility of wild-type FAT10 upon binding with NUB1 (the shorter splice variant of NUB1L) using hydrogen-deuterium exchange detected by mass spectrometry.[53] In the absence of NUB1, several peptides from both the N- and the C-domain show a bimodal distribution, indicating coexisting folded and unfolded states. In the presence of NUB1, peptides throughout the N-domain were exposed, except for the last β5-strand. Thus, NUB1 traps an unfolded state of the N-domain of FAT10. The coexistence of folded and unfolded states may well explain the troubles encountered in the investigation of the N-domain of FAT10 by liquid-state NMR. Theng *et al.* were only successful after deletion of the first seven N-terminal residues and even then residues P59-T73 could not be detected by ^{1}H-^{15}N heteronuclear single-quantum correlation (HSQC); in the structure they obtained, the α1-helix is somewhat displaced (PDB-ID 2MBE).[11]

Arkinson *et al.* found their conclusion supported by structure prediction with AlphaFold-Multimer and by site-directed mutagenesis: FAT10 mutants H75A, H75D and H75K compromised NUB1 binding, H75D and H75K also abolished degradation.[53] Cao *et al.* recently went a step further showing that phosphorylation of T77 interferes with NUB1L binding.[55] Interestingly, Arkinson *et al.* detected no complex formation between full-length Cys-free FAT10 and NUB1, while in our hands complex formation between N-FAT10-C0 and NUB1L is evident (Figure S1). Possibly

the absence of the C-domain makes it easier for the N-domain to become inserted into the clasp of NUB1L. Finally, Arkinson *et al.* showed by cryo-electron microscopy that FAT10 binding induces an open conformation of NUB1, allowing its ubiquitin-like (UBL) domain to interact with the RPN1 subunit[56] of the regulatory particle for direct FAT10 delivery. In spite of directed efforts, however, it was not possible to resolve the interaction of NUB1 with FAT10.

Structure-based sequence alignment of FAT10 with ubiquitin reveals two extra residues in the N-domain preceding the β5-strand (K70, E71), extending the loop. Molecular dynamics simulations indicate loose folding in this region[21], in agreement with the experimental observations by MAS NMR. Moreover, multiple sequence alignment of mammalian FAT10 proteins reveals a highly conserved surface comprising residues T73, H75, L76, T77, L78, and V80. This region of N-FAT10 thus seems primed for formation of the intermolecular β-sheet with NUB1L. This is reminiscent of the capture of an unstructured β-strand degron by two Catch subdomains in the midnolin pathway of ubiquitin-independent protein degradation.[57] In the case of N-FAT10, the primed region appears to constitute an interaction motif. Titrations in combination with liquid-state NMR have implicated the β1- and β5-strands of N-FAT10 in the binding with MAD2.[11] MAD2, in turn, is known to undergo β-sheet augmentation with reshuffling upon complex formation with CDC20 (cell-division-control protein 20) or MAD1.[58] This interaction motif, however, brings the risk of aggregation. In β2-microglobulin, the pathogenic D76N mutation destabilizes protective edge β-strands, which exposes aggregation-prone regions and enables amyloid formation.[59]

In biomolecular MAS NMR, the observation of a residue is indicative of slow dynamics associated with a regular, stable structure. In the case of the complex of N-FAT10-C0 and NUB1L, this applies to residues I68-V81, of which T73-V81 form a β-strand, the N-terminus (G4), and eleven more residues of which we could sequentially assign only W17 (there is just one Trp in the sequence). The other, unobserved residues of N-FAT10-C0 are disordered and quite possibly dynamic on micro- to millisecond time scales – motion in this intermediate regime tends to make both J-coupling and dipolar-coupling based experiments inefficient. Integrated approaches of MAS NMR, liquid-state NMR, and molecular dynamics simulations, have demonstrated such dynamic disorder in enzymes, its connection to structural frustration, and the functional importance.[60,61] Based on the MAS NMR data and the AlphaFold-Multimer prediction (see below) we propose that NUB1L and N-FAT10 form a fuzzy complex[62] in which NUB1L is the predominantly folded "reverse chaperone" and N-FAT10 is the predominantly unfolded client. The two proteins interact via the intermolecular β-sheet and via electrostatic and hydrophobic interactions at the scattered, non-sequentially assigned residues. The N-terminus of N-FAT10 binds to NUB1L in a yet-unknown location.

AlphaFold-Multimer predicts with high confidence that the β2-strand and α1-helix of N-FAT10-C0 remain partially intact (Figures 5c, S11), but this is not reflected in the MAS NMR spectra. This likely relates to the known tendency of AlphaFold to predict, for intrinsically disordered proteins or regions, the structures of conditionally folded states, i.e., stable structures that form under specific conditions such as the interaction with a binding partner or following post-translational modification.[63] For example, AlphaFold's predicted structure of isolated 4E-BP2 simultaneously contains the four β-strand structure that forms upon multisite phosphorylation[64] and two helices that resemble those observed in crystal structures of 4E-BP2 and 4E-BP1 bound to translation initiator factor 4E.[65,66] The prediction of the intact β2-strand and α1-helix is thus likely a remnant of the conditional folding of isolated N-FAT10-C0. There is additional disagreement between AlphaFold-Multimer and the MAS NMR data regarding the length of the

intermolecular β-sheet. AlphaFold-Multimer predicts residues L76-V81 of N-FAT10-C0 to participate whereas TALOS-N classifies T73-V81 as β-strand. This is not just due to the rendering of the secondary structure: the backbone torsion angles of I74 are clearly distinct (TALOS-N: $\Phi = -133.3°$, $\Psi = 155.3°$; AlphaFold-Multimer/VADAR: $\Phi = -117.1°$, $\Psi = -24.2°$, see Figure S10). To accommodate the longer β-sheet, NUB1L would have to undergo a conformational change. Finally, AlphaFold-Multimer does not predict the interactions of NUB1L with the scattered anchor residues of N-FAT10-C0, including the N-terminus. All this emphasizes that experimental data remain essential in the investigation of the structures and functions of weakly folded proteins. MAS NMR experiments that could shed more light on the interaction of N-FAT10 and NUB1L include frequency-selective rotational-echo double-resonance (REDOR)[67] to measure specific ^{13}C-^{15}N distances, the double-REDOR filter[68] to identify intermolecular interfaces, ^{1}H detection enabled by ultrafast MAS[69] to explore the hydrogen bonding network of the anti-parallel β-sheet, and relaxation dispersion[70] to probe microsecond time-scale conformational fluctuations.

CONCLUSION

We have reported the MAS NMR investigation of the ubiquitin-like modifier FAT10 and its interaction with adapter protein NUB1L. Sequential assignment of amino acid residues followed by empirical prediction of torsion angles and secondary structure has provided insight into the biological function of the weak folding of FAT10. When the N-domain of FAT10 is in the ubiquitin-like β-grasp fold, residues I68 through (approximately) V80 constitute a partially unstructured degron. In preparation of rapid degradation by the proteasome, NUB1L stabilizes the N-domain of FAT10 in a mostly unfolded state. Residues I68-V81 attain structural homogeneity and so do a number of anchor residues, including the N-terminus. Chemical shifts indicate that residues T73-V81 form a β-strand, providing experimental, structural evidence for β-strand capture in ubiquitin-independent protein degradation. The binding of the N-terminus, presumably to NUB1L, likely plays a critical role in the presentation of the unfolded N-FAT10 chain to the proteasome.

ASSOCIATED CONTENT

Supporting Information. Protocols for N-FAT10-C0 and NUB1L expression and purification; preparation of samples for MAS NMR, including size-exclusion chromatography and SDS-PAGE showing complex formation of N-FAT10-C0 and NUB1L; MAS NMR spectroscopy: overview of all experiments and acquisition parameters; ^{1}H-^{15}N cross-polarization spectra; ^{13}C-^{13}C and ^{15}N-^{13}C spectra of microcrystalline N-FAT10-C0 and visualization of secondary structure predictions; strip plot of microcrystalline N-FAT10-C0; strip plots of lyophilized/rehydrated N-FAT10-C0; torsion angle analysis of lyophilized/rehydrated N-FAT10-C0; strip plot of N-FAT10-C0 in complex with NUB1L; temperature dependence of N-FAT10-C0 in complex with NUB1L; torsion angle analysis of N-FAT10-C0 in complex with NUB1L; AlphaFold-Multimer confidence scores. This material is available free of charge via the Internet at http://pubs.acs.org.

Data availability. All data generated in this study have been deposited in the Zenodo repository.

AUTHOR INFORMATION

Corresponding Author

*Guinevere Mathies – Department of Chemistry, University of Konstanz, Konstanz 78464, Germany; E-mail: guinevere.mathies@uni-konstanz.de

Author Contributions

All authors have given approval to the final version of the manuscript.

Notes

The authors declare no competing financial interest.

Acknowledgments

This research was funded by the Deutsche Forschungsgemeinschaft through the Emmy Noether Program (Project No. 321027114), SFB 969 (Project No. 189682160), and SFB 1527 (Project No. 454252029) and by the Swiss National Science Foundation (Projects No. 201070 and 219514). The authors thank Michael Kovermann, Ulrich Haunz, and Anke Friemel for maintenance of the NMR instrumentation, Venkata SubbaRao Redrouthu for support with the measurements, Leon Schöwe and Gunter Schmidtke for support in the biolab, Salima Bahri for practical advice, and Stefan Gerlach for support regarding the Scientific Compute Cluster at the University of Konstanz (SCCKN).

References

(1) Fan, W.; Cai, W.; Parimoo, S.; Lennon, G. G.; Weissman, S. M. Identification of Seven New Human MHC Class I Region Genes around the HLA-F Locus. *Immunogenetics* **1996**, *44* (2), 97–103. https://doi.org/10.1007/BF02660056.

(2) Bates, E. E. M.; Ravel, O.; Dieu, M.-C.; Ho, S.; Guret, C.; Bridon, J.-M.; Ait-Yahia, S.; Brière, F.; Caux, C.; Banchereau, J.; Lebecque, S. Identification and Analysis of a Novel Member of the Ubiquitin Family Expressed in Dendritic Cells and Mature B Cells. *Eur. J. Immunol.* **1997**, *27* (10), 2471–2477. https://doi.org/10.1002/eji.1830271002.

(3) Lukasiak, S.; Schiller, C.; Oehlschlaeger, P.; Schmidtke, G.; Krause, P.; Legler, D. F.; Autschbach, F.; Schirmacher, P.; Breuhahn, K.; Groettrup, M. Proinflammatory Cytokines Cause FAT10 Upregulation in Cancers of Liver and Colon. *Oncogene* **2008**, *27* (46), 6068–6074. https://doi.org/10.1038/onc.2008.201.

(4) Schregle, R.; Mah, M. M.; Mueller, S.; Aichem, A.; Basler, M.; Groettrup, M. The Expression Profile of the Ubiquitin-like Modifier FAT10 in Immune Cells Suggests Cell Type-Specific Functions. *Immunogenetics* **2018**, *70* (7), 429–438. https://doi.org/10.1007/s00251-018-1055-5.

(5) Liu, Y. C.; Pan, J.; Zhang, C.; Fan, W.; Collinge, M.; Bender, J. R.; Weissman, S. M. A MHC-Encoded Ubiquitin-like Protein (FAT10) Binds Noncovalently to the Spindle Assembly Checkpoint Protein MAD2. *Proc. Natl. Acad. Sci. U. S. A.* **1999**, *96* (8), 4313–4318. https://doi.org/10.1073/pnas.96.8.4313.

(6) Raasi, S.; Schmidtke, G.; de Giuli, R.; Groettrup, M. A Ubiquitin-like Protein Which Is Synergistically Inducible by Interferon-Gamma and Tumor Necrosis Factor-Alpha. *Eur J Immunol* **1999**, *29* (12), 4030–4036. https://doi.org/10.1002/(sici)1521-4141(199912)29:12<4030::Aid-immu4030>3.0.Co;2-y.

(7) Ebstein, F.; Lehmann, A.; Kloetzel, P.-M. The FAT10- and Ubiquitin-Dependent Degradation Machineries Exhibit Common and Distinct Requirements for MHC Class I Antigen Presentation. *Cell. Mol. Life Sci. CMLS* **2012**, *69* (14), 2443–2454. https://doi.org/10.1007/s00018-012-0933-5.

(8) Aichem, A.; Kalveram, B.; Spinnenhirn, V.; Kluge, K.; Catone, N.; Johansen, T.; Groettrup, M. The Proteomic Analysis of Endogenous FAT10 Substrates Identifies P62/SQSTM1 as a Substrate of FAT10ylation. *J. Cell Sci.* **2012**, *125* (19), 4576–4585. https://doi.org/10.1242/jcs.107789.

(9) Aichem, A.; Groettrup, M. The Ubiquitin-like Modifier FAT10 – Much More than a Proteasome-Targeting Signal. *J. Cell Sci.* **2020**, *133* (14), jcs246041. https://doi.org/10.1242/jcs.246041.

(10) Lee, C. G. L.; Ren, J.; Cheong, I. S. Y.; Ban, K. H. K.; Ooi, L. L. P. J.; Yong Tan, S.; Kan, A.; Nuchprayoon, I.; Jin, R.; Lee, K.-H.; Choti, M.; Lee, L. A. Expression of the FAT10 Gene Is Highly Upregulated in Hepatocellular Carcinoma and Other Gastrointestinal and Gynecological Cancers. *Oncogene* **2003**, *22* (17), 2592–2603. https://doi.org/10.1038/sj.onc.1206337.

(11) Theng, S. S.; Wang, W.; Mah, W.-C.; Chan, C.; Zhuo, J.; Gao, Y.; Qin, H.; Lim, L.; Chong, S. S.; Song, J.; Lee, C. G. Disruption of FAT10–MAD2 Binding Inhibits Tumor Progression. *Proc. Natl. Acad. Sci.* **2014**, *111* (49). https://doi.org/10.1073/pnas.1403383111.

(12) Hipp, M. S.; Kalveram, B.; Raasi, S.; Groettrup, M.; Schmidtke, G. FAT10, a Ubiquitin-Independent Signal for Proteasomal Degradation. *Mol. Cell. Biol.* **2005**, *25* (9), 3483–3491. https://doi.org/10.1128/MCB.25.9.3483-3491.2005.

(13) Chiu, Y.-H.; Sun, Q.; Chen, Z. J. E1-L2 Activates Both Ubiquitin and FAT10. *Mol. Cell* **2007**, *27* (6), 1014–1023. https://doi.org/10.1016/j.molcel.2007.08.020.

(14) Groettrup, M.; Pelzer, C.; Schmidtke, G.; Hofmann, K. Activating the Ubiquitin Family: UBA6 Challenges the Field. *Trends Biochem. Sci.* **2008**, *33* (5), 230–237. https://doi.org/10.1016/j.tibs.2008.01.005.

(15) Aichem, A.; Pelzer, C.; Lukasiak, S.; Kalveram, B.; Sheppard, P. W.; Rani, N.; Schmidtke, G.; Groettrup, M. USE1 Is a Bispecific Conjugating Enzyme for Ubiquitin and FAT10, Which FAT10ylates Itself in Cis. *Nat. Commun.* **2010**, *1* (1), 13. https://doi.org/10.1038/ncomms1012.

(16) Schnell, L.; Zubrod, A.; Catone, N.; Bialas, J.; Aichem, A. Tumor Necrosis Factor Mediates USE1-Independent FAT10ylation under Inflammatory Conditions. *Life Sci. Alliance* **2023**, *6* (11), e202301985. https://doi.org/10.26508/lsa.202301985.

(17) Roverato, N. D.; Sailer, C.; Catone, N.; Aichem, A.; Stengel, F.; Groettrup, M. Parkin Is an E3 Ligase for the Ubiquitin-like Modifier FAT10, Which Inhibits Parkin Activation and Mitophagy. *Cell Rep.* **2021**, *34* (11), 108857. https://doi.org/10.1016/j.celrep.2021.108857.

(18) Hipp, M. S.; Raasi, S.; Groettrup, M.; Schmidtke, G. NEDD8 Ultimate Buster-1L Interacts with the Ubiquitin-like Protein FAT10 and Accelerates Its Degradation. *J. Biol. Chem.* **2004**, *279* (16), 16503–16510. https://doi.org/10.1074/jbc.M310114200.

(19) Schmidtke, G.; Kalveram, B.; Groettrup, M. Degradation of FAT10 by the 26S Proteasome Is Independent of Ubiquitylation but Relies on NUB1L. *FEBS Lett.* **2009**, *583* (3), 591–594. https://doi.org/10.1016/j.febslet.2009.01.006.

(20) Brockmann, F.; Catone, N.; Wünsch, C.; Offensperger, F.; Scheffner, M.; Schmidtke, G.; Aichem, A. FAT10 and NUB1L Cooperate to Activate the 26S Proteasome. *Life Sci. Alliance* **2023**, *6* (8), e202201463. https://doi.org/10.26508/lsa.202201463.

(21) Aichem, A.; Anders, S.; Catone, N.; Rößler, P.; Stotz, S.; Berg, A.; Schwab, R.; Scheuermann, S.; Bialas, J.; Schütz-Stoffregen, M. C.; Schmidtke, G.; Peter, C.; Groettrup, M.; Wiesner, S. The Structure of the Ubiquitin-like Modifier FAT10 Reveals an Alternative Targeting Mechanism for Proteasomal Degradation. *Nat. Commun.* **2018**, *9* (1), 3321. https://doi.org/10.1038/s41467-018-05776-3.

(22) Buchsbaum, S.; Bercovich, B.; Ziv, T.; Ciechanover, A. Modification of the Inflammatory Mediator LRRFIP2 by the Ubiquitin-like Protein FAT10 Inhibits Its Activity during Cellular Response to LPS. *Biochem. Biophys. Res. Commun.* **2012**, *428* (1), 11–16. https://doi.org/10.1016/j.bbrc.2012.09.110.

(23) Nguyen, N. T. H.; Now, H.; Kim, W.-J.; Kim, N.; Yoo, J.-Y. Ubiquitin-like Modifier FAT10 Attenuates RIG-I Mediated Antiviral Signaling by Segregating Activated RIG-I from Its Signaling Platform. *Sci. Rep.* **2016**, *6* (1), 23377. https://doi.org/10.1038/srep23377.

(24) Vijay-Kumar, S.; Bugg, C. E.; Cook, W. J. Structure of Ubiquitin Refined at 1.8 Å Resolution. *J. Mol. Biol.* **1987**, *194* (3), 531–544. https://doi.org/10.1016/0022-2836(87)90679-6.

(25) Guo, C.; Alfaro-Aco, R.; Zhang, C.; Russell, R. W.; Petry, S.; Polenova, T. Structural Basis of Protein Condensation on Microtubules Underlying Branching Microtubule Nucleation. *Nat. Commun.* **2023**, *14* (1), 3682. https://doi.org/10.1038/s41467-023-39176-z.

(26) El Mammeri, N.; Duan, P.; Hong, M. Pseudo-Phosphorylated Tau Forms Paired Helical Filaments in the Presence of High-Curvature Cholesterol-Containing Lipid Membranes. *J. Am. Chem. Soc.* **2025**, *147* (3), 2510–2522. https://doi.org/10.1021/jacs.4c13772.

(27) Barbet-Massin, E.; Huang, C.; Daebel, V.; Hsu, S. D.; Reif, B. Site-Specific Solid-State NMR Studies of “Trigger Factor” in Complex with the Large Ribosomal Subunit 50S. *Angew. Chem. Int. Ed.* **2015**, *54* (14), 4367–4369. https://doi.org/10.1002/anie.201409393.

(28) Gardiennet, C.; Wiegand, T.; Bazin, A.; Cadalbert, R.; Kunert, B.; Lacabanne, D.; Gutsche, I.; Terradot, L.; Meier, B. H.; Böckmann, A. Solid-State NMR Chemical-Shift Perturbations Indicate Domain Reorientation of the DnaG Primase in the Primosome of Helicobacter Pylori. *J. Biomol. NMR* **2016**, *64* (3), 189–195. https://doi.org/10.1007/s10858-016-0018-0.

(29) Evans, R.; O'Neill, M.; Pritzel, A.; Antropova, N.; Senior, A.; Green, T.; Žídek, A.; Bates, R.; Blackwell, S.; Yim, J.; Ronneberger, O.; Bodenstein, S.; Zielinski, M.; Bridgland, A.; Potapenko, A.; Cowie, A.; Tunyasuvunakool, K.; Jain, R.; Clancy, E.; Kohli, P.; Jumper, J.; Hassabis, D. Protein Complex Prediction with AlphaFold-Multimer. *bioRxiv* **2022**, 2021.10.04.463034. https://doi.org/10.1101/2021.10.04.463034.

(30) Mandal, A.; Boatz, J. C.; Wheeler, T. B.; Van Der Wel, P. C. A. On the Use of Ultracentrifugal Devices for Routine Sample Preparation in Biomolecular Magic-Angle-Spinning NMR. *J. Biomol. NMR* **2017**, *67* (3), 165–178. https://doi.org/10.1007/s10858-017-0089-6.

(31) Bertini, I.; Luchinat, C.; Parigi, G.; Ravera, E. SedNMR: On the Edge between Solution and Solid-State NMR. *Acc. Chem. Res.* **2013**, *46* (9), 2059–2069. https://doi.org/10.1021/ar300342f.

(32) Schmidtke, G.; Kalveram, B.; Weber, E.; Bochtler, P.; Lukasiak, S.; Hipp, M. S.; Groettrup, M. The UBA Domains of NUB1L Are Required for Binding but Not for Accelerated Degradation of the Ubiquitin-like Modifier FAT10. *J. Biol. Chem.* **2006**, *281* (29), 20045–20054. https://doi.org/10.1074/jbc.M603063200.

(33) Takegoshi, K.; Nakamura, S.; Terao, T. ^{13}C–^{1}H Dipolar-Assisted Rotational Resonance in Magic-Angle Spinning NMR. *Chem. Phys. Lett.* **2001**, *344* (5–6), 631–637. https://doi.org/10.1016/S0009-2614(01)00791-6.

(34) Jaroniec, C. P.; Filip, C.; Griffin, R. G. 3D TEDOR NMR Experiments for the Simultaneous Measurement of Multiple Carbon−Nitrogen Distances in Uniformly ^{13}C,^{15}N-Labeled Solids. *J. Am. Chem. Soc.* **2002**, *124* (36), 10728–10742. https://doi.org/10.1021/ja026385y.

(35) Daviso, E.; Eddy, M. T.; Andreas, L. B.; Griffin, R. G.; Herzfeld, J. Efficient Resonance Assignment of Proteins in MAS NMR by Simultaneous Intra- and Inter-Residue 3D Correlation Spectroscopy. *J. Biomol. NMR* **2013**, *55* (3), 257–265. https://doi.org/10.1007/s10858-013-9707-0.

(36) Andreas, L. B.; Eddy, M. T.; Chou, J. J.; Griffin, R. G. Magic-Angle-Spinning NMR of the Drug Resistant S31N M2 Proton Transporter from Influenza A. *J. Am. Chem. Soc.* **2012**, *134* (17), 7215–7218. https://doi.org/10.1021/ja3003606.

(37) Baldus, M.; Petkova, A. T.; Herzfeld, J.; Griffin, R. G. Cross Polarization in the Tilted Frame: Assignment and Spectral Simplification in Heteronuclear Spin Systems. *Mol. Phys.* **1998**, *95* (6), 1197–1207. https://doi.org/10.1080/00268979809483251.

(38) Hou, G.; Yan, S.; Trébosc, J.; Amoureux, J.-P.; Polenova, T. Broadband Homonuclear Correlation Spectroscopy Driven by Combined R2nv Sequences under Fast Magic Angle Spinning for NMR Structural Analysis of Organic and Biological Solids. *J. Magn. Reson.* **2013**, *232*, 18–30. https://doi.org/10.1016/j.jmr.2013.04.009.

(39) Delaglio, F.; Grzesiek, S.; Vuister, G. W.; Zhu, G.; Pfeifer, J.; Bax, A. NMRPipe: A Multidimensional Spectral Processing System Based on UNIX Pipes. *J. Biomol. NMR* **1995**, *6* (3), 277–293. https://doi.org/10.1007/BF00197809.

(40) Skinner, S. P.; Fogh, R. H.; Boucher, W.; Ragan, T. J.; Mureddu, L. G.; Vuister, G. W. CcpNmr AnalysisAssign: A Flexible Platform for Integrated NMR Analysis. *J. Biomol. NMR* **2016**, *66* (2), 111–124. https://doi.org/10.1007/s10858-016-0060-y.

(41) Higman, V. A. Solid-State MAS NMR Resonance Assignment Methods for Proteins. *Prog. Nucl. Magn. Reson. Spectrosc.* **2018**, *106–107*, 37–65. https://doi.org/10.1016/j.pnmrs.2018.04.002.

(42) Wishart, D. S.; Sykes, B. D.; Richards, F. M. Relationship between Nuclear Magnetic Resonance Chemical Shift and Protein Secondary Structure. *J. Mol. Biol.* **1991**, *222* (2), 311–333. https://doi.org/10.1016/0022-2836(91)90214-Q.

(43) Spera, S.; Bax, A. Empirical Correlation between Protein Backbone Conformation and C.Alpha. and C.Beta. 13C Nuclear Magnetic Resonance Chemical Shifts. *J. Am. Chem. Soc.* **1991**, *113* (14), 5490–5492. https://doi.org/10.1021/ja00014a071.

(44) Shen, Y.; Bax, A. Protein Backbone and Sidechain Torsion Angles Predicted from NMR Chemical Shifts Using Artificial Neural Networks. *J. Biomol. NMR* **2013**, *56* (3), 227–241. https://doi.org/10.1007/s10858-013-9741-y.

(45) Jumper, J.; Evans, R.; Pritzel, A.; Green, T.; Figurnov, M.; Ronneberger, O.; Tunyasuvunakool, K.; Bates, R.; Žídek, A.; Potapenko, A.; Bridgland, A.; Meyer, C.; Kohl, S. A. A.; Ballard, A. J.; Cowie, A.; Romera-Paredes, B.; Nikolov, S.; Jain, R.; Adler, J.; Back, T.; Petersen, S.; Reiman, D.; Clancy, E.; Zielinski, M.; Steinegger, M.; Pacholska, M.; Berghammer, T.; Silver, D.; Vinyals, O.; Senior, A. W.; Kavukcuoglu, K.; Kohli, P.; Hassabis, D. Applying and Improving AlphaFold at CASP14. *Proteins Struct. Funct. Bioinforma.* **2021**, *89* (12), 1711–1721. https://doi.org/10.1002/prot.26257.

(46) Meng, E. C.; Goddard, T. D.; Pettersen, E. F.; Couch, G. S.; Pearson, Z. J.; Morris, J. H.; Ferrin, T. E. UCSF ChimeraX: Tools for Structure Building and Analysis. *Protein Sci.* **2023**, *32* (11), e4792. https://doi.org/10.1002/pro.4792.

(47) Willard, L. VADAR: A Web Server for Quantitative Evaluation of Protein Structure Quality. *Nucleic Acids Res.* **2003**, *31* (13), 3316–3319. https://doi.org/10.1093/nar/gkg565.

(48) Martin, R. W.; Zilm, K. W. Preparation of Protein Nanocrystals and Their Characterization by Solid State NMR. *J. Magn. Reson.* **2003**, *165* (1), 162–174. https://doi.org/10.1016/S1090-7807(03)00253-2.

(49) Kraus, J.; Sarkar, S.; Quinn, C. M.; Polenova, T. Solid-State NMR Spectroscopy of Microcrystalline Proteins. In *Annual Reports on NMR Spectroscopy*; Elsevier, 2021; Vol. 102, pp 81–151. https://doi.org/10.1016/bs.arnmr.2020.10.002.

(50) Frericks Schmidt, H. L.; Shah, G. J.; Sperling, L. J.; Rienstra, C. M. NMR Determination of Protein p K_a Values in the Solid State. *J. Phys. Chem. Lett.* **2010**, *1* (10), 1623–1628. https://doi.org/10.1021/jz1004413.

(51) Platzer, G.; Okon, M.; McIntosh, L. P. pH-Dependent Random Coil 1H, 13C, and 15N Chemical Shifts of the Ionizable Amino Acids: A Guide for Protein pK a Measurements. *J. Biomol. NMR* **2014**, *60* (2–3), 109–129. https://doi.org/10.1007/s10858-014-9862-y.

(52) Morris, G. A.; Freeman, R. Enhancement of Nuclear Magnetic Resonance Signals by Polarization Transfer. *J. Am. Chem. Soc.* **1979**, *101* (3), 760–762. https://doi.org/10.1021/ja00497a058.

(53) Arkinson, C.; Dong, K. C.; Gee, C. L.; Costello, S. M.; Soe, A. C.; Hura, G. L.; Marqusee, S.; Martin, A. NUB1 Traps Unfolded FAT10 for Ubiquitin-Independent Degradation by the 26S Proteasome. *Nat. Struct. Mol. Biol.* **2025**. https://doi.org/10.1038/s41594-025-01527-3.

(54) Truongvan, N.; Li, S.; Misra, M.; Kuhn, M.; Schindelin, H. Structures of UBA6 Explain Its Dual Specificity for Ubiquitin and FAT10. *Nat. Commun.* **2022**, *13* (1), 4789. https://doi.org/10.1038/s41467-022-32040-6.

(55) Cao, J.; Aichem, A.; Basler, M.; Alvarez Salinas, G. O.; Schmidtke, G. Phosphorylated FAT10 Is More Efficiently Conjugated to Substrates, Does Not Bind to NUB1L, and Does Not Alter Degradation by the Proteasome. *Biomedicines* **2024**, *12* (12), 2795.

(56) Rani, N.; Aichem, A.; Schmidtke, G.; Kreft, S. G.; Groettrup, M. FAT10 and NUB1L Bind to the VWA Domain of Rpn10 and Rpn1 to Enable Proteasome-Mediated Proteolysis. *Nat. Commun.* **2012**, *3* (1), 749. https://doi.org/10.1038/ncomms1752.

(57) Gu, X.; Nardone, C.; Kamitaki, N.; Mao, A.; Elledge, S. J.; Greenberg, M. E. The Midnolin-Proteasome Pathway Catches Proteins for Ubiquitination-Independent Degradation. *Science* **2023**, *381* (6660), eadh5021. https://doi.org/10.1126/science.adh5021.

(58) Remaut, H.; Waksman, G. Protein–Protein Interaction through β-Strand Addition. *Trends Biochem. Sci.* **2006**, *31* (8), 436–444. https://doi.org/10.1016/j.tibs.2006.06.007.

(59) Le Marchand, T.; De Rosa, M.; Salvi, N.; Sala, B. M.; Andreas, L. B.; Barbet-Massin, E.; Sormanni, P.; Barbiroli, A.; Porcari, R.; Sousa Mota, C.; De Sanctis, D.; Bolognesi, M.; Emsley, L.; Bellotti, V.; Blackledge, M.; Camilloni, C.; Pintacuda, G.; Ricagno, S. Conformational Dynamics in Crystals Reveal the Molecular Bases for D76N Beta-2 Microglobulin Aggregation Propensity. *Nat. Commun.* **2018**, *9* (1). https://doi.org/10.1038/s41467-018-04078-y.

(60) Gauto, D. F.; Macek, P.; Malinverni, D.; Fraga, H.; Paloni, M.; Sučec, I.; Hessel, A.; Bustamante, J. P.; Barducci, A.; Schanda, P. Functional Control of a 0.5 MDa TET Aminopeptidase by a Flexible Loop Revealed by MAS NMR. *Nat. Commun.* **2022**, *13* (1). https://doi.org/10.1038/s41467-022-29423-0.

(61) Troussicot, L.; Vallet, A.; Molin, M.; Burmann, B. M.; Schanda, P. Disulfide-Bond-Induced Structural Frustration and Dynamic Disorder in a Peroxiredoxin from MAS NMR. *J. Am. Chem. Soc.* **2023**, *145* (19), 10700–10711. https://doi.org/10.1021/jacs.3c01200.

(62) Tompa, P.; Fuxreiter, M. Fuzzy Complexes: Polymorphism and Structural Disorder in Protein–Protein Interactions. *Trends Biochem. Sci.* **2008**, *33* (1), 2–8. https://doi.org/10.1016/j.tibs.2007.10.003.

(63) Alderson, T. R.; Pritišanac, I.; Kolarić, Đ.; Moses, A. M.; Forman-Kay, J. D. Systematic Identification of Conditionally Folded Intrinsically Disordered Regions by AlphaFold2. *Proc. Natl. Acad. Sci.* **2023**, *120* (44). https://doi.org/10.1073/pnas.2304302120.

(64) Bah, A.; Vernon, R. M.; Siddiqui, Z.; Krzeminski, M.; Muhandiram, R.; Zhao, C.; Sonenberg, N.; Kay, L. E.; Forman-Kay, J. D. Folding of an Intrinsically Disordered Protein by Phosphorylation as a Regulatory Switch. *Nature* **2015**, *519* (7541), 106–109. https://doi.org/10.1038/nature13999.

(65) Fukuyo, A.; In, Y.; Ishida, T.; Tomoo, K. Structural Scaffold for eIF4E Binding Selectivity of 4E-BP Isoforms: Crystal Structure of eIF4E Binding Region of 4E-BP2 and Its Comparison with That of 4E-BP1. *J. Pept. Sci.* **2011**, *17* (9), 650–657. https://doi.org/10.1002/psc.1384.

(66) Sekiyama, N.; Arthanari, H.; Papadopoulos, E.; Rodriguez-Mias, R. A.; Wagner, G.; Léger-Abraham, M. Molecular Mechanism of the Dual Activity of 4EGI-1: Dissociating eIF4G from eIF4E but Stabilizing the Binding of Unphosphorylated 4E-BP1. *Proc. Natl. Acad. Sci.* **2015**, *112* (30). https://doi.org/10.1073/pnas.1512118112.

(67) Jaroniec, C. P.; Tounge, B. A.; Herzfeld, J.; Griffin, R. G. Frequency Selective Heteronuclear Dipolar Recoupling in Rotating Solids: Accurate ^{13}C–^{15}N Distance Measurements in Uniformly ^{13}C,^{15}N-Labeled Peptides. *J. Am. Chem. Soc.* **2001**, *123* (15), 3507–3519. https://doi.org/10.1021/ja003266e.

(68) Guo, C.; Hou, G.; Lu, X.; Polenova, T. Mapping Protein–Protein Interactions by Double-REDOR-Filtered Magic Angle Spinning NMR Spectroscopy. *J. Biomol. NMR* **2017**, *67* (2), 95–108. https://doi.org/10.1007/s10858-016-0086-1.

(69) Le Marchand, T.; Schubeis, T.; Bonaccorsi, M.; Paluch, P.; Lalli, D.; Pell, A. J.; Andreas, L. B.; Jaudzems, K.; Stanek, J.; Pintacuda, G. ^{1}H-Detected Biomolecular NMR under Fast Magic-Angle Spinning. *Chem. Rev.* **2022**, *122* (10), 9943–10018. https://doi.org/10.1021/acs.chemrev.1c00918.

(70) Rovó, P. Recent Advances in Solid-State Relaxation Dispersion Techniques. *Solid State Nucl. Magn. Reson.* **2020**, *108*, 101665. https://doi.org/10.1016/j.ssnmr.2020.101665.